Analytical Center of Mass Trajectory Generation for Humanoid Walking and Running with Continuous Gait Transitions

Tobias Egle, Johannes Englsberger, and Christian Ott

***Abstract*— We present an analytical trajectory generation framework for the combined computation of multiple walking and running sequences with continuous gait transitions. This framework builds on the Divergent Component of Motion (DCM)-based walking algorithm and the spline-based trajectory generation of the Biologically Inspired Deadbeat (BID) control for running. We describe our approach to generating closed-form center of mass (CoM) trajectories for walking and running by alternately linking the two gaits through continuity constraints. Thereby, we distinguish between vertical and horizontal planning. The vertical trajectory is computed in a forward recursion from the first to the last gait sequence. Due to the coupling of the gait sequences in the horizontal direction, we show the efficient generation of the horizontal CoM trajectory in a single matrix calculation. Subsequently, we unify the control strategies using a DCM tracking controller for the complete trajectory and integrate the proposed framework into an inverse dynamics-based whole-body controller. Finally, the presented approaches are validated in simulations with the humanoid robot Toro.**

I. Introduction

Bipedal locomotion promises improved accessibility and navigation of complex and non-barrier-free terrain compared to wheel-based mobility. However, this versatility has the disadvantage of generally achieving slower locomotion speeds. In contrast to most of today's humanoid robots, humans can significantly increase their locomotion speed by changing their gait from walking to running.

Non-human-like locomotion machines are capable of high speeds [1] and powerful jumps [2] but are highly specialized. For humanoid robots designed for versatility, running is still challenging due to the short, potentially underactuated contacts and the high torque demands on the joints. Furthermore, the biomechanics of walking and running differ significantly. In walking, the body's center of mass (CoM) reaches a maximal height in the middle of the stance phase, while the opposite is true for running [3]. Usually, different mathematical models and control strategies are adopted to reproduce the CoM motions for the two gaits.

Most scientific works in robotic bipedal locomotion follow the idea of focusing on the robot's CoM dynamics for generating gait trajectories. One of the most popular models for *walking* is the Linear Inverted Pendulum (LIP) model [5]–[7]. In this approach, the CoM acceleration can be completely described by the position of the zero moment point (ZMP) relative to the CoM. The ZMP is defined as a point on the ground where the horizontal moments of contact forces around the CoM are zero. Using the concept of the Divergent Component of Motion (DCM) introduced by [8], the second-order CoM dynamics can be separated into stable and unstable components. As a generalization of the capture point (or 2D DCM) [9]–[11], Englsberger et al. [12] extended this concept to 3D with the introduction of the Virtual Repellent Point (VRP). In this formulation, the CoM naturally converges to the DCM (stable dynamics), and the DCM diverges away from the VRP (unstable dynamics). By embedding the DCM-based walking controller into a whole-body control framework, stable walking motion was shown in simulation and experiments on the humanoid Toro.

The generation of *running* trajectories is commonly based on switching dynamical constraints between the stance and flight phases. In the stance phase, approaches similar to walking using the LIP model are adopted to generate a running pattern [13]–[15]. Other studies utilize the Spring-Loaded Inverted Pendulum (SLIP) model, which consists of a point mass on top of a massless, compliant leg. With appropriate parameters and initial conditions, the SLIP model can be shown to be open-loop stable [16] or can be controlled to return to a stable limit cycle [17]–[19]. However, there are no closed-form solutions for the SLIP model. This motivates

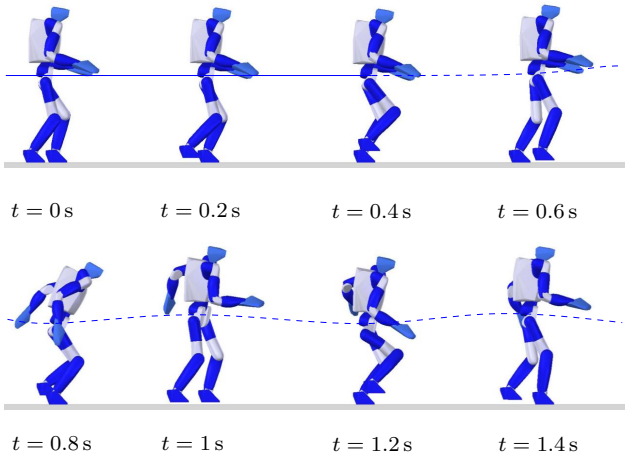

Fig. 1. Time series of the humanoid robot Toro [4] in simulation during the walk-to-run (W2R) transition with CoM motion indicated (continuous line: walking, dashed line: running).

Tobias Egle and Christian Ott are with the Automation and Control Institute, Faculty of Electrical Engineering and Information Technology, TU Wien, 1040 Vienna, Austria tobias.egle@tuwien.ac.at, christian.ott@tuwien.ac.at

Johannes Englsberger is with the Institute of Robotics and Mechatronics, German Aerospace Center (DLR), 82234 Wessling, Germany johannes.englsberger@dlr.de

This project has received funding from the European Research Council (ERC) under the European Union's Horizon 2020 research and innovation programme (grant agreement No. 819358)

 DOI: 10.1109/Humanoids53995.2022.10000236

the approach by [20], which aims to use polynomial splines to design CoM trajectories that produce approximately natural ground reaction forces by fulfilling a set of boundary conditions. This trajectory planner is utilized to construct a deadbeat controller, the so-called Biologically Inspired Deadbeat (BID) controller, and integrated into an inverse dynamics-based whole-body control framework to produce stable full-body running motion in simulation.

A variety of approaches are used for the *transition between walking and running*. Rummel et al. [21] found overlaps between stable limit cycles of walking and running, showing that the same locomotion speed can be achieved with both gaits, and [22] discretely changes the locomotion mode between walking, running, and hopping for push recovery. Similar to the VRP approach, Sugihara et al. [23] enhanced the ZMP model to 3D, which can represent variations of the CoM height and enables seamless transitions between walking and running without pre-planning the overall trajectory. Most recently, Smaldone et al. [24] used an MPC approach to realize transitions between walking and running.

The main contribution of this paper is the introduction of a combined analytical trajectory generation for walking and running, which allows to pre-plan a complete multi-step motion reference. We show that the proposed method merges two distinctly different planning approaches for walking [12] and running [20] into a single framework. Together with a unified control approach, we achieve smooth transitions between standing, walking, and running in a whole-body simulation. The paper is organized as follows. Section II introduces the two trajectory generation concepts for walking and running. Section III presents our approach for the combined trajectory generation of the two gaits separately for the vertical direction (Section III-A) and horizontal directions (Section III-B). We evaluate the proposed methods in a whole-body simulation with the humanoid robot TORO in Section IV, and Section V concludes the paper.

II. Preliminaries

A. DCM-based Trajectory Generation for Walking

The trajectory generation for walking is based on the concepts of three-dimensional Divergent Component of Motion (DCM) and Virtual Repellent Point (VRP), introduced in [25]. Here, the DCM $\boldsymbol{\xi}$ is defined as a linear combination of the CoM position $\boldsymbol{x}$ and velocity $\dot{\boldsymbol{x}}$ as

$$\boldsymbol{\xi} = \boldsymbol{x} + b\dot{\boldsymbol{x}}, \tag{1}$$

where the time constant $b = \sqrt{\Delta z / g_z}$ is determined by the average height of the CoM over the ground Δz and the gravitational constant g_z. The total force $\boldsymbol{f}$ on the CoM is encoded by the VRP $\boldsymbol{v}$ as

$$\boldsymbol{f} = \frac{m}{b^2}\left(\boldsymbol{x} - \boldsymbol{v}\right), \tag{2}$$

where m is the total mass. This force-to-point transformation simplifies handling the robot's hybrid dynamics by allowing discrete foot positions to be mapped to VRP waypoints, from which a VRP trajectory is generated by piecewise interpolation. We find the DCM dynamics by differentiating (1) and inserting the CoM dynamics $\ddot{\boldsymbol{x}} = \boldsymbol{f}/m$ with (2) as

$$\dot{\boldsymbol{\xi}} = \frac{1}{b}\left(\boldsymbol{\xi} - \boldsymbol{v}\right). \tag{3}$$

To generate DCM and CoM trajectories, the walking motion is split into n_φ transition phases. We choose a DCM target point $\boldsymbol{\xi}_f$ and a CoM start point $\boldsymbol{x}_s$ as boundary conditions for the complete motion. By specifying a VRP trajectory $\boldsymbol{v}_\varphi(t)$ for each transition phase φ, we can solve (1) and (3) with appropriate initial and terminal values to obtain the DCM trajectory $\boldsymbol{\xi}_\varphi(t)$ and CoM trajectory $\boldsymbol{x}_\varphi(t)$ (for details see [26]). We denote $\boldsymbol{v}_\varphi(0) = \boldsymbol{v}_{\varphi,0}$ as the VRP phase start points and $\boldsymbol{v}_\varphi(T_\varphi) = \boldsymbol{v}_{\varphi,T}$ as the VRP phase end points, where T_φ is the phase duration, and equivalently define the DCM and CoM start and end points. To ensure continuity of the complete trajectory, the transition phase start and end points of adjacent phases are linked, i.e. $\boldsymbol{v}_{\varphi,0} = \boldsymbol{v}_{\varphi-1,T}$, $\boldsymbol{\xi}_{\varphi,0} = \boldsymbol{\xi}_{\varphi-1,T}$ and $\boldsymbol{x}_{\varphi,0} = \boldsymbol{x}_{\varphi-1,T}$. Thus a complete VRP, DCM and CoM trajectory can be described as a piecewise interpolation of $n = n_\varphi + 1$ VRP waypoints $\boldsymbol{V} = [\boldsymbol{v}_1 \dots \boldsymbol{v}_n]^\mathrm{T}$, DCM waypoints $\boldsymbol{\Xi} = [\boldsymbol{\xi}_1 \dots \boldsymbol{\xi}_n]^\mathrm{T}$ and CoM waypoints $\boldsymbol{X} = [\boldsymbol{x}_1 \dots \boldsymbol{x}_n]^\mathrm{T}$, respectively. An efficient computation of the DCM and CoM waypoints can be summarized to

$$\begin{bmatrix} \boldsymbol{X} \\ \boldsymbol{\Xi} \end{bmatrix} = \underbrace{\begin{bmatrix} {}^X\boldsymbol{c}_x & {}^X\boldsymbol{c}_\xi \\ \boldsymbol{0} & {}^\Xi\boldsymbol{c}_\xi \end{bmatrix}}_{\boldsymbol{A}_W} \begin{bmatrix} \boldsymbol{x}_s^\mathrm{T} \\ \boldsymbol{\xi}_f^\mathrm{T} \end{bmatrix} + \underbrace{\begin{bmatrix} {}^X\boldsymbol{C}_V \\ {}^\Xi\boldsymbol{C}_V \end{bmatrix}}_{\boldsymbol{B}_W} \boldsymbol{V}, \tag{4}$$

where the detailed analytical computation of the components of $\boldsymbol{A}_W$ and $\boldsymbol{B}_W$ can be found in [26]. The backward mapping for the DCM is chosen due to its increased numeric stability compared to a forward mapping.

B. Spline-based Trajectory Generation for Running

In [20], a biologically inspired running trajectory generation was introduced as part of the BID framework to design CoM trajectories that produce approximately natural ground reaction forces (GRF). It was shown that human GRF profiles could be approximated by a second-order polynomial in the vertical direction and third-order polynomials in the horizontal directions. This corresponds to the CoM position being expressed by fourth-order polynomials in the vertical direction and fifth-order polynomials in the horizontal direction. The polynomial encoding is given by

$$\begin{bmatrix} \sigma(t) \\ \dot{\sigma}(t) \\ \ddot{\sigma}(t) \end{bmatrix} = \begin{bmatrix} 1 & t & t^2 & t^3 & t^4 & t^5 \\ 0 & 1 & 2t & 3t^2 & 4t^3 & 5t^4 \\ 0 & 0 & 2 & 6t & 12t^2 & 20t^3 \end{bmatrix} \boldsymbol{p}_\sigma = \begin{bmatrix} \boldsymbol{t}_\sigma^\mathrm{T} \\ \boldsymbol{t}_{\dot{\sigma}}^\mathrm{T} \\ \boldsymbol{t}_{\ddot{\sigma}}^\mathrm{T} \end{bmatrix} \boldsymbol{p}_\sigma, \tag{5}$$

where $\sigma \in \{x, y, z\}$. The last components of $\boldsymbol{t}_\sigma^\mathrm{T}$, $\boldsymbol{t}_{\dot{\sigma}}^\mathrm{T} = d/dt\ \boldsymbol{t}_\sigma^\mathrm{T} = \dot{\boldsymbol{t}}_\sigma^\mathrm{T}$ and $\boldsymbol{t}_{\ddot{\sigma}}^\mathrm{T}$ are grayed out to indicate that they are used only for the horizontal directions. The running motion is divided into n stance phases and corresponding flight phases.

1) Vertical planning: For each stance phase i (duration $T_{s,i}$), four linear vertical boundary conditions for five pa-

rameters $\boldsymbol{p}_{z,i} \in \mathbb{R}^5$ are determined as

$$\underbrace{\begin{bmatrix} z_{\mathrm{TD},i} \\ \dot{z}_{\mathrm{TD},i} \\ -g_z \\ -g_z \end{bmatrix}}_{\boldsymbol{b}_{z,i}} = \underbrace{\begin{bmatrix} \boldsymbol{t}_z^{\mathrm{T}}(0) \\ \boldsymbol{t}_{\dot{z}}^{\mathrm{T}}(0) \\ \boldsymbol{t}_{\ddot{z}}^{\mathrm{T}}(0) \\ \boldsymbol{t}_{\ddot{z}}^{\mathrm{T}}(T_{s,i}) \end{bmatrix}}_{\boldsymbol{B}_{z,i}} \boldsymbol{p}_{z,i}. \tag{6}$$

Here, the first element in $\boldsymbol{b}_{z,i}$ specifies the CoM height at the start of the stance phase (touchdown, TD) and the last two elements imply that the stance phase's initial and terminal CoM acceleration equals minus gravity, i.e., the vertical leg force is zero. The general solution of (6) is given by

$$\boldsymbol{p}_{z,i} = \underbrace{\boldsymbol{B}_{z,i}^{\mathrm{T}} \left(\boldsymbol{B}_{z,i}\, \boldsymbol{B}_{z,i}^{\mathrm{T}} \right)^{-1} \boldsymbol{b}_{z,i}}_{\boldsymbol{p}_{z,i,0}} + \boldsymbol{r}_{z,i}\, \tilde{p}_{z,i}, \tag{7}$$

where $\boldsymbol{r}_{z,i}$ spans the one-dimensional nullspace of $\boldsymbol{B}_{z,i}$. With the remaining degree of freedom $\tilde{p}_{z,i}$, we aim to achieve the desired apex height of the next flight phase. The stance time $T_{s,i}$, apex height and TD height are design parameters of the planning approach (for details, see [20]).

2) Horizontal planning: For each stance phase i, five linear horizontal boundary conditions for six polynomial parameters $\boldsymbol{P}_{\chi,i} \in \mathbb{R}^{6\times 2}$ (rows for x and y) are defined as

$$\underbrace{\begin{bmatrix} \boldsymbol{\chi}_{\mathrm{TD},i} \\ \dot{\boldsymbol{\chi}}_{\mathrm{TD},i} \\ \mathbf{0} \\ \mathbf{0} \\ \boldsymbol{\chi}_{\mathrm{ft},i} \end{bmatrix}}_{\boldsymbol{H}_{\chi,i}} = \underbrace{\begin{bmatrix} \boldsymbol{t}_{\chi}^{\mathrm{T}}(0) \\ \boldsymbol{t}_{\dot{\chi}}^{\mathrm{T}}(0) \\ \boldsymbol{t}_{\ddot{\chi}}^{\mathrm{T}}(0) \\ \boldsymbol{t}_{\ddot{\chi}}^{\mathrm{T}}(T_{s,i}) \\ \boldsymbol{l}_{\chi,i}^{\mathrm{T}} \end{bmatrix}}_{\boldsymbol{B}_{\chi,i}} \boldsymbol{P}_{\chi,i}. \tag{8}$$

In general, the vector $\boldsymbol{\chi} = [x\ y]$ summarizes horizontal positions. Here, the first element in $\boldsymbol{H}_{\chi,i}$ specifies the horizontal CoM position at the start of the stance phase. The third and fourth elements imply that the stance phase's initial and terminal acceleration equals zero, i.e., horizontal leg forces are zero. In the last row of $\boldsymbol{B}_{\chi,i}$, the vector $\boldsymbol{l}_{\chi,i}^{\mathrm{T}}$ maps the polynomial parameters to the foot positions $\boldsymbol{\chi}_{\mathrm{ft},i}$ (see [20], where $\boldsymbol{l}_{\chi,i}^{\mathrm{T}}$ is denoted as $\boldsymbol{e}_{\chi,i}^{\mathrm{T}}$). The general solution of (8) is analogous to (7). With the remaining degrees of freedom $\tilde{\boldsymbol{p}}_{\chi,i}^{*} = [\tilde{p}_{x,i}\ \tilde{p}_{y,i}] \in \mathbb{R}^2$, we aim to provide the best possible focus of leg forces at the foot target position. The solution for (8) is found as

$$\boldsymbol{P}_{\chi,i} = \underbrace{\left(\boldsymbol{I} - \frac{\boldsymbol{r}_{\chi,i}\, \boldsymbol{r}_{\chi,i}^{\mathrm{T}}\, \boldsymbol{M}_{\chi,i}}{\boldsymbol{r}_{\chi,i}^{\mathrm{T}}\, \boldsymbol{M}_{\chi,i}\, \boldsymbol{r}_{\chi,i}} \right)}_{\boldsymbol{\Omega}_{\chi,i}} \underbrace{\boldsymbol{B}_{\chi,i}^{\mathrm{T}} \left(\boldsymbol{B}_{\chi,i}\, \boldsymbol{B}_{\chi,i}^{\mathrm{T}} \right)^{-1}}_{\boldsymbol{B}_{\chi,i}^{+}} \boldsymbol{H}_{\chi,i}. \tag{9}$$

For details on the analytical computation of the polynomial parameters $\boldsymbol{P}_{\chi,i}$ and matrix $\boldsymbol{M}_{\chi,i}$, see [20].

III. Combining Trajectory Generation for Walking and Running

In this section, we propose a method to combine the planning of walking and running trajectories by transforming the corresponding equations of the running gait generation to enable the linkage of the two gaits through continuity constraints. We do not change the trajectory generation methods or introduce additional design parameters. Similar to the division of walking into transition phases and running into stance and flight phases, we divide the overall motion into N_g gait sequences and assume it always starts and ends with walking[1] (i.e., N_g is odd). In this paper, we use basis vectors of different lengths to define selectors. Thus, we denote with $\boldsymbol{e}_{\ell,i}$ the i-th basis vector of $\mathbb{R}^{\ell}$. To simplify notation, we assume that each walking and running sequence consists of n waypoints and stance phases, respectively.

As shown in the previous section, the planning methods for each gait sequence $g \in \{1 \dots N_g\}$ differ significantly. However, enforcing continuity of position, velocity, and acceleration suffice to ensure smooth gait transitions. Thus, we define three continuity conditions for each gait transition:

$$\boldsymbol{x}_{1,g} = \boldsymbol{x}_{n,g-1}, \tag{10}$$

$$\dot{\boldsymbol{x}}_{1,g} = \dot{\boldsymbol{x}}_{n,g-1}, \tag{11}$$

$$\ddot{\boldsymbol{x}}_{1,g} = \ddot{\boldsymbol{x}}_{n,g-1}, \tag{12}$$

for all $g \in \{2, 3, \dots, N_g\}$, where $\boldsymbol{x}_{1,g}$ is the *first* position waypoint in gait sequence g and $\boldsymbol{x}_{n,g-1}$ is the *last* position waypoint in the previous gait sequence $g-1$. For a combined calculation of walking and running gaits, we agree on the quantities of walking, i.e., CoM $\boldsymbol{x}$, DCM $\boldsymbol{\xi}$, and VRP $\boldsymbol{v}$, as common variables for the continuity conditions. We use a DCM position and CoM velocity terminal condition for each walking and running[2] sequence, respectively, to ensure stability of the trajectory. Hence, we transform the velocity continuity condition (11) with (1) to a DCM continuity constraint and reformulate as a backward recursive equation:

$$\boldsymbol{\xi}_{n,g} = \boldsymbol{\xi}_{1,g+1} \quad \forall g \in \{1, 2, \dots, N_g - 1\}, \tag{13}$$

where $\boldsymbol{\xi}_{n,g}$ is the last DCM waypoint in gait sequence g and $\boldsymbol{\xi}_{1,g+1}$ is the first DCM waypoint in the next gait sequence $g+1$. For each walking sequence, the VRP trajectory depends on the robot's foot positions and can be predetermined. By inserting (2) divided by the total mass m into (12), we find that the acceleration continuity condition is fulfilled by continuity of the CoM position (10) and a continuity requirement on the VRP trajectory. We satisfy this constraint by choosing the first and last VRP waypoints in running as

$$\boldsymbol{v}_{1,g} = \boldsymbol{v}_{n,g-1} \quad \forall g \in g_r, \tag{14}$$

$$\boldsymbol{v}_{n,g} = \boldsymbol{v}_{1,g+1} \quad \forall g \in g_r. \tag{15}$$

Here, the set $g_r = \{2, 4, \dots, N_g - 1\}$ contains the even indices of the running sequences. Additionally, we denote with $g_w = \{1, 3, \dots, N_g\}$ the set of odd walking sequence indices. Consequently, two continuity conditions remain, i.e. (10) and (13), which must be satisfied alternately by walking or running. Equivalently to a single walking sequence, we

[1] The gait transition can be performed in the footstep after the initial and before the final double support phase, respectively.

[2] The terminal condition exists only for the horizontal planning in running.

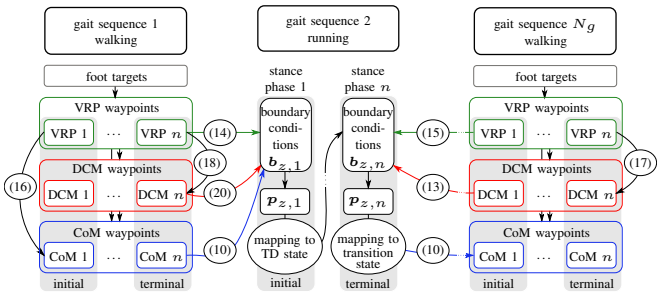

Fig. 2. Outline of the *vertical* planning computation flow

choose a global CoM start point $\bar{\boldsymbol{x}}_s$ and DCM target point $\bar{\boldsymbol{\xi}}_f$ in the first and last gait sequence, respectively, as

$$\bar{\boldsymbol{x}}_s = \boldsymbol{v}_{1,1}, \tag{16}$$

$$\bar{\boldsymbol{\xi}}_f = \boldsymbol{v}_{n,N_g}. \tag{17}$$

With these inputs, the entire trajectory can be represented as a function of the foot targets and VRP waypoints, which are themselves a function of the foot targets. Since the horizontal and vertical trajectory for running is calculated separately, we maintain this separation for the combined computation.

A. Vertical Planning of Walking and Running

This section presents the computation of the *vertical* trajectory for multiple walking and running sequences. The computation flow is outlined in Fig. 2 and illustrates the continuity conditions between the gait phases, which are described in more detail below.

1) Walking: Each walking sequence g depends on both the preceding and the succeeding gait sequence. By choosing the final vertical DCM position in (4) to coincide with the respective last vertical VRP position, i.e.,

$$\xi_{z,n,g} = v_{z,n,g}, \tag{18}$$

we can resolve the dependence on the next gait sequence in the vertical direction (this assumption is valid as the TD height is a design variable in running). With (18) and the third row of (10), we write (4) for the vertical direction and gait sequence g as

$$\begin{bmatrix} \boldsymbol{z}_g \\ \boldsymbol{\xi}_{z,g} \end{bmatrix} = \begin{bmatrix} {}^{X}\boldsymbol{c}_x \\ \boldsymbol{0} \end{bmatrix} z_{n,g-1} + \begin{bmatrix} {}^{X}\boldsymbol{c}_{\xi,g}\boldsymbol{e}_{n,n}^{\mathrm{T}} + {}^{X}\boldsymbol{C}_{V,g} \\ {}^{\Xi}\boldsymbol{c}_{\xi,g}\boldsymbol{e}_{n,n}^{\mathrm{T}} + {}^{\Xi}\boldsymbol{C}_{V,g} \end{bmatrix} \boldsymbol{v}_{z,g}. \tag{19}$$

Here, the second row only depends on $\boldsymbol{v}_{z,g}$. Thus, we can calculate the DCM waypoints for all walking sequences in advance and independent of the running sequences. The vertical component of the CoM waypoints still depends on the last CoM position waypoint of the previous gait sequence. With the third row of (16), we can calculate the vertical CoM waypoints in a forward recursion, as shown in Fig. 2.

2) Running: For all but the first and last stance phases of each running sequence, the boundary conditions consist of (6). In contrast, we must adjust the boundary conditions in the first and last stance phase to connect the trajectory generation for running to the walking sequences. As the terminal value for walking is fixed in (18), we need a continuity constraint for the initial DCM position as

$$\xi_{z,1,g} = \xi_{z,n,g-1} \quad \forall g \in g_r. \tag{20}$$

In the first stance phase, we use (1) and (2) divided by m to transform the CoM velocity to DCM and CoM acceleration to VRP continuity conditions, respectively, and insert (20) and the third rows of (10) and (14) as

$$\underbrace{\begin{bmatrix} z_{n,g-1} \\ \xi_{z,n,g-1} \\ v_{z,n,g-1} \\ -g \end{bmatrix}}_{\boldsymbol{b}_{z,1}} = \underbrace{\begin{bmatrix} \boldsymbol{t}_z^{\mathrm{T}}(0) \\ \boldsymbol{t}_z^{\mathrm{T}}(0) + b\,\boldsymbol{t}_{\dot{z}}^{\mathrm{T}}(0) \\ \boldsymbol{t}_z^{\mathrm{T}}(0) - b^2\,\boldsymbol{t}_{\ddot{z}}^{\mathrm{T}}(0) \\ \boldsymbol{t}_{\ddot{z}}^{\mathrm{T}}(T_{s,1}) \end{bmatrix}}_{\boldsymbol{B}_{z,1}} \boldsymbol{p}_{z,1}. \tag{21}$$

Here, the last boundary condition remains unchanged as it specifies the acceleration at the end of the first stance phase.

While the first three boundary conditions of (6) remain unchanged in the final stance phase, the fourth boundary condition is replaced by a VRP continuity condition. Additionally, we introduce a terminal DCM boundary condition for the final stance phase that replaces the non-linear apex height boundary condition. The five linear boundary and continuity conditions in the final stance phase are given by

$$\underbrace{\begin{bmatrix} z_{\mathrm{TD},n} \\ \dot{z}_{\mathrm{TD},n} \\ -g \\ v_{z,1,g+1} \\ \xi_{z,1,g+1} \end{bmatrix}}_{\boldsymbol{b}_{z,n}} = \underbrace{\begin{bmatrix} \boldsymbol{t}_z^{\mathrm{T}}(0) \\ \boldsymbol{t}_{\dot{z}}^{\mathrm{T}}(0) \\ \boldsymbol{t}_{\ddot{z}}^{\mathrm{T}}(0) \\ \boldsymbol{t}_z^{\mathrm{T}}(T_{s,n}) - b^2\,\boldsymbol{t}_{\ddot{z}}^{\mathrm{T}}(T_{s,n}) \\ \boldsymbol{t}_z^{\mathrm{T}}(T_{s,n}) + b\,\boldsymbol{t}_{\dot{z}}^{\mathrm{T}}(T_{s,n}) \end{bmatrix}}_{\boldsymbol{B}_{z,n}} \boldsymbol{p}_{z,n}. \tag{22}$$

Here, with five boundary conditions and five polynomial parameters $\boldsymbol{p}_{z,n}$, the square, full-rank matrix $\boldsymbol{B}_{z,n}$ is invertible. The detailed calculation of the waypoints is shown in [20].

B. Horizontal Planning of Walking and Running

In *horizontal* planning, we avoid constraining the last DCM position, so the coupling to the preceding and succeeding gait sequence remains. Therefore, we need to solve for all gait sequence waypoints in a combined computation. First, our goal is to obtain a mapping between gait sequence initial and terminal waypoints and the respective foot targets for each gait sequence g as indicated in Fig. 3. Secondly, by using these equations, we assemble a global matrix equation to compute the initial and terminal waypoints for all gait sequences in terms of foot positions, the global CoM start point $\bar{\boldsymbol{x}}_s$ and DCM target point $\bar{\boldsymbol{\xi}}_f$.

1) Walking: The horizontal VRP and foot positions coincide. Thus, we find a compact expression of the VRP waypoints (VRP stationary in foot center during single support) in terms of foot positions for gait sequence g as

$$\boldsymbol{V}_{\chi,g} = \boldsymbol{B}_{f,g}\boldsymbol{X}_{\mathrm{ft},g}, \tag{23}$$

where $\boldsymbol{B}_f \in \mathbb{R}^{n\times n_t}$ is a block diagonal matrix whose diagonal contains the matrices $\boldsymbol{b}_{f,k} = [1\ \ 1]^{\mathrm{T}}$, $k \in \{1 \dots n_t\}$, and n_t is the total number of foot targets. This equation is generally valid except for the stationary initial and terminal

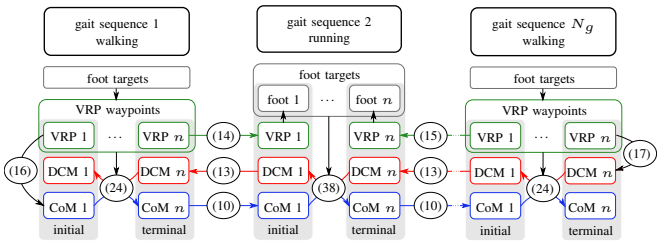

Fig. 3. Outline of the *horizontal* planning computation scheme

double support phase. Equation (4) shows the calculation of all CoM and DCM waypoints. To obtain the mapping to the last CoM position $\boldsymbol{\chi}_{n,g}$ and first DCM position $\boldsymbol{\xi}_{\chi,1,g}$, we select the corresponding rows in (4) and insert (23) as

$$\begin{aligned}\begin{bmatrix}\boldsymbol{\chi}_{n,g}\\ \boldsymbol{\xi}_{\chi,1,g}\end{bmatrix} &= \begin{bmatrix}\boldsymbol{e}_{n,n}^{\mathrm{T}} & \boldsymbol{0}\\ \boldsymbol{0} & \boldsymbol{e}_{n,1}^{\mathrm{T}}\end{bmatrix}\left(\boldsymbol{A}_W\begin{bmatrix}\boldsymbol{\chi}_{1,g}\\ \boldsymbol{\xi}_{\chi,n,g}\end{bmatrix}+\boldsymbol{B}_W\boldsymbol{B}_{f,g}\boldsymbol{X}_{\mathrm{ft},g}\right)\\ &= \begin{bmatrix}{}^{\chi}a_{\chi,g} & {}^{\chi}a_{\xi,g}\\ 0 & {}^{\xi}a_{\xi,g}\end{bmatrix}\begin{bmatrix}\boldsymbol{\chi}_{1,g}\\ \boldsymbol{\xi}_{\chi,n,g}\end{bmatrix}+\begin{bmatrix}{}^{\chi}\boldsymbol{b}_{t,g}\\ {}^{\xi}\boldsymbol{b}_{t,g}\end{bmatrix}\boldsymbol{X}_{\mathrm{ft},g}.\end{aligned} \tag{24}$$

This yields the mapping between the initial and terminal waypoints and the foot positions of walking, which is later used to assemble the global matrix equation.

2) Running: In this section, the waypoints of the running trajectory are computed efficiently in a matrix equation, which is subsequently transformed to resemble the common structure shown in (24) for walking. The takeoff (TO) state at the end of each running stance phase i is defined as

$$\underbrace{\begin{bmatrix}\boldsymbol{\chi}_{\mathrm{TO},i}\\ \dot{\boldsymbol{\chi}}_{\mathrm{TO},i}\end{bmatrix}}_{\boldsymbol{S}_{\mathrm{TO},i}} = \underbrace{\begin{bmatrix}\boldsymbol{t}_{\chi}^{\mathrm{T}}(T_{s,i})\\ \boldsymbol{t}_{\dot{\chi}}^{\mathrm{T}}(T_{s,i})\end{bmatrix}}_{\boldsymbol{T}_{\chi,i}}\boldsymbol{P}_{\chi,i}. \tag{25}$$

We insert (9) into (25) as

$$\boldsymbol{S}_{\mathrm{TO},i} = \underbrace{\boldsymbol{T}_{\chi,i}\boldsymbol{\Omega}_{\chi,i}\boldsymbol{B}_{\chi,i}^{+}}_{\boldsymbol{D}_{\chi,i}\in\mathbb{R}^{2\times 5}}\boldsymbol{H}_{\chi,i}. \tag{26}$$

Combining the first two columns in $\boldsymbol{D}_{\chi,i}$ and separating the remaining columns allows (26) to be extended to

$$\boldsymbol{S}_{\mathrm{TO},i} = \boldsymbol{D}_{\alpha,i}\underbrace{\begin{bmatrix}\boldsymbol{\chi}_{\mathrm{TD},i}\\ \dot{\boldsymbol{\chi}}_{\mathrm{TD},i}\end{bmatrix}}_{\boldsymbol{S}_{\mathrm{TD},i}}+\boldsymbol{d}_{\beta,i}\ddot{\boldsymbol{\chi}}_{\mathrm{TD},i}+\boldsymbol{d}_{\gamma,i}\ddot{\boldsymbol{\chi}}_{\mathrm{TO},i}+\boldsymbol{d}_{\delta,i}\boldsymbol{\chi}_{\mathrm{ft},i}, \tag{27}$$

where $\boldsymbol{D}_{\alpha,i}$ summarizes the first two columns and $\boldsymbol{d}_{\beta,i}$, $\boldsymbol{d}_{\gamma,i}$, and $\boldsymbol{d}_{\delta,i}$ denote the third, fourth, and fifth columns of $\boldsymbol{D}_{\chi,i}$, respectively. For all running stance phases, we assemble the TD state $\boldsymbol{S}_{\mathrm{TD},i}$, TO state $\boldsymbol{S}_{\mathrm{TO},i}$ and foot positions $\boldsymbol{\chi}_{\mathrm{ft},i}$ in the TD state matrix $\boldsymbol{S}_{\mathrm{TD}} = [\boldsymbol{S}_{\mathrm{TD},1}^{\mathrm{T}}\cdots\boldsymbol{S}_{\mathrm{TD},n}^{\mathrm{T}}]^{\mathrm{T}}$, the TO state matrix $\boldsymbol{S}_{\mathrm{TO}} = [\boldsymbol{S}_{\mathrm{TO},1}^{\mathrm{T}}\cdots\boldsymbol{S}_{\mathrm{TO},n}^{\mathrm{T}}]^{\mathrm{T}}$ and the foot position matrix $\boldsymbol{X}_{\mathrm{ft}} = [\boldsymbol{\chi}_{\mathrm{ft},1}^{\mathrm{T}}\cdots\boldsymbol{\chi}_{\mathrm{ft},n_t}^{\mathrm{T}}]^{\mathrm{T}}$, respectively. In each running sequence, there are two acceleration waypoints in the transition to walking that are not equal to zero, i.e., the first TD acceleration $\ddot{\boldsymbol{\chi}}_{\mathrm{TD},1}$ and last TO acceleration $\ddot{\boldsymbol{\chi}}_{\mathrm{TO},n}$[3].

[3]Note that there is no actual TD and TO in the first and last stance phase of running due to the transition from and to walking, respectively. However, the quantities are still indicated as TO/TD for consistency of notation.

All other acceleration waypoints are zero, and the respective boundary conditions are implicitly satisfied. We write (27) in matrix form for all n running stance phases as

$$\boldsymbol{S}_{\mathrm{TO}} = \boldsymbol{D}_{\alpha}\boldsymbol{S}_{\mathrm{TD}}+\boldsymbol{D}_{\beta}\ddot{\boldsymbol{\chi}}_{\mathrm{TD},1}+\boldsymbol{D}_{\gamma}\ddot{\boldsymbol{\chi}}_{\mathrm{TO},n}+\boldsymbol{D}_{\delta}\boldsymbol{X}_{\mathrm{ft}}, \tag{28}$$

where $\boldsymbol{D}_{\beta} = \boldsymbol{Z}_1^{\mathrm{T}}\boldsymbol{d}_{\beta,1}$, $\boldsymbol{D}_{\gamma} = \boldsymbol{Z}_N^{\mathrm{T}}\boldsymbol{d}_{\gamma,n}$ and $\boldsymbol{D}_{\alpha}$ and $\boldsymbol{D}_{\delta}$ are block diagonal matrices whose diagonal contains the single-phase matrices $\boldsymbol{D}_{\alpha,i}$ and vectors $\boldsymbol{d}_{\delta,i}$, respectively. The selection matrices $\boldsymbol{Z}_1 = [\boldsymbol{e}_{2n,1}\ \boldsymbol{e}_{2n,2}]^{\mathrm{T}}$ and $\boldsymbol{Z}_N = [\boldsymbol{e}_{2n,2n-1}\ \boldsymbol{e}_{2n,2n}]^{\mathrm{T}}$ select the first and last state from the state matrices $\boldsymbol{S}_{\mathrm{TO}}$ and $\boldsymbol{S}_{\mathrm{TD}}$. Additionally, we introduce the selection matrix $\boldsymbol{Z}_T = [\boldsymbol{e}_{2n,3}\dots\boldsymbol{e}_{2n,2n}]^{\mathrm{T}}$, which selects the states $2\dots n$ from the state matrices ($\boldsymbol{S}_{\mathrm{TD}}$ and $\boldsymbol{S}_{\mathrm{TO}}$) and denote with $\boldsymbol{S}_{\mathrm{TD},T} = \boldsymbol{Z}_T\boldsymbol{S}_{\mathrm{TD}}$ the corresponding states. Thus, we can separate the mapping of the first TD state $\boldsymbol{S}_{\mathrm{TD},1}$ to the TO state matrix $\boldsymbol{S}_{\mathrm{TO}}$ in (28) as

$$\begin{aligned}\boldsymbol{S}_{\mathrm{TO}} = \boldsymbol{Z}_1^{\mathrm{T}}\boldsymbol{D}_{\alpha,1}\boldsymbol{S}_{\mathrm{TD},1}+\boldsymbol{D}_{\alpha}\boldsymbol{Z}_T^{\mathrm{T}}\boldsymbol{S}_{\mathrm{TD},T}\\ +\boldsymbol{D}_{\delta}\boldsymbol{X}_{\mathrm{ft}}+\boldsymbol{D}_{\beta}\ddot{\boldsymbol{\chi}}_{\mathrm{TD},1}+\boldsymbol{D}_{\gamma}\ddot{\boldsymbol{\chi}}_{\mathrm{TO},n}.\end{aligned} \tag{29}$$

Here, $\boldsymbol{Z}_1^{\mathrm{T}}\boldsymbol{D}_{\alpha,1}$ are the first two columns and $\boldsymbol{D}_{\alpha}\boldsymbol{Z}_T^{\mathrm{T}}$ are all remaining columns of $\boldsymbol{D}_{\alpha}$. In the flight phase, we compute the upcoming TD state in terms of the TO state as

$$\underbrace{\begin{bmatrix}\boldsymbol{\chi}_{\mathrm{TD},i+1}\\ \dot{\boldsymbol{\chi}}_{\mathrm{TD},i+1}\end{bmatrix}}_{\boldsymbol{S}_{\mathrm{TD},i+1}} = \underbrace{\begin{bmatrix}1 & T_{f,i}\\ 0 & 1\end{bmatrix}}_{\boldsymbol{A}_{F,i}}\underbrace{\begin{bmatrix}\boldsymbol{\chi}_{\mathrm{TO},i}\\ \dot{\boldsymbol{\chi}}_{\mathrm{TO},i}\end{bmatrix}}_{\boldsymbol{S}_{\mathrm{TO},i}}, \tag{30}$$

for all $i\in\{1\dots n-1\}$. We write in matrix form for all running phases n as

$$\boldsymbol{S}_{\mathrm{TD},T} = \boldsymbol{A}_F\boldsymbol{Z}_0\boldsymbol{S}_{\mathrm{TO}}, \tag{31}$$

where $\boldsymbol{A}_F$ is a block diagonal matrix whose diagonal contains the single flight phase mapping matrices $\boldsymbol{A}_{F,i}$ and the selection matrix $\boldsymbol{Z}_0 = [\boldsymbol{e}_{2n,1}\dots\boldsymbol{e}_{2n,2n-2}]^{\mathrm{T}}$ selects the states $1\dots n-1$ from the state matrices $\boldsymbol{S}_{\mathrm{TD}}$ and $\boldsymbol{S}_{\mathrm{TO}}$. We insert (31) into (29) and solve for $\boldsymbol{S}_{\mathrm{TO}}$ as

$$\boldsymbol{S}_{\mathrm{TO}} = \boldsymbol{D}_R\big(\boldsymbol{Z}_1^{\mathrm{T}}\boldsymbol{D}_{\alpha,1}\boldsymbol{S}_{\mathrm{TD},1}+\boldsymbol{D}_{\delta}\boldsymbol{X}_{\mathrm{ft}}+\boldsymbol{D}_{\beta}\ddot{\boldsymbol{\chi}}_{\mathrm{TD},1}+\boldsymbol{D}_{\gamma}\ddot{\boldsymbol{\chi}}_{\mathrm{TO},n}\big), \tag{32}$$

where $\boldsymbol{D}_R = (\boldsymbol{I}-\boldsymbol{D}_{\alpha}\boldsymbol{Z}_T^{\mathrm{T}}\boldsymbol{A}_F\boldsymbol{Z}_0)^{-1}$. This is valid as the matrix $\boldsymbol{D}_R^{-1}$ is a lower triangular matrix with non-zero elements on the diagonal and thus invertible. By selecting the last two rows of (32), we obtain the final TO state as

$$\begin{aligned}\boldsymbol{S}_{\mathrm{TO},n} = \boldsymbol{Z}_N\boldsymbol{D}_R\boldsymbol{Z}_1^{\mathrm{T}}\boldsymbol{D}_{\alpha,1}\boldsymbol{S}_{\mathrm{TD},1}+\boldsymbol{Z}_N\boldsymbol{D}_R\boldsymbol{D}_{\delta}\boldsymbol{X}_{\mathrm{ft}}\\ +\boldsymbol{Z}_N\boldsymbol{D}_R\boldsymbol{D}_{\beta}\ddot{\boldsymbol{\chi}}_{\mathrm{TD},1}+\boldsymbol{Z}_N\boldsymbol{D}_R\boldsymbol{D}_{\gamma}\ddot{\boldsymbol{\chi}}_{\mathrm{TO},n}.\end{aligned} \tag{33}$$

This yields the mapping between running initial and terminal waypoints and foot positions, which must be transformed to the coordinates of the walking trajectory. Reordering, we augment the final TO state and first TD state by their respective CoM accelerations and write for gait sequence g:

$$\begin{aligned}\underbrace{\begin{bmatrix}\boldsymbol{I}_{2\times 2} & -\boldsymbol{Z}_N\boldsymbol{D}_R\boldsymbol{D}_{\gamma}\end{bmatrix}}_{\boldsymbol{A}_{N,g}}\begin{bmatrix}\boldsymbol{S}_{\mathrm{TO},n,g}\\ \ddot{\boldsymbol{\chi}}_{\mathrm{TO},n,g}\end{bmatrix} = \underbrace{\boldsymbol{Z}_N\boldsymbol{D}_R\boldsymbol{D}_{\delta}}_{\boldsymbol{A}_{T,g}}\boldsymbol{X}_{\mathrm{ft},g}+\\ \underbrace{\begin{bmatrix}\boldsymbol{Z}_N\boldsymbol{D}_R\boldsymbol{Z}_1\boldsymbol{D}_{\alpha,1} & \boldsymbol{Z}_N\boldsymbol{D}_R\boldsymbol{D}_{\beta}\end{bmatrix}}_{\boldsymbol{A}_{1,g}}\begin{bmatrix}\boldsymbol{S}_{\mathrm{TD},1,g}\\ \ddot{\boldsymbol{\chi}}_{\mathrm{TD},1,g}\end{bmatrix}.\end{aligned} \tag{34}$$

To obtain the identical coordinates for walking and running, we introduce the coordinate transformation for the final augmented TO state for gait sequence g as

$$\begin{bmatrix} \boldsymbol{\chi}_{\mathrm{TO},n,g} \\ \dot{\boldsymbol{\chi}}_{\mathrm{TO},n,g} \\ \ddot{\boldsymbol{\chi}}_{\mathrm{TO},n,g} \end{bmatrix} = \underbrace{\begin{bmatrix} 1 \\ -1/b \\ 1/b^2 \end{bmatrix}}_{\boldsymbol{h}_\chi} \underbrace{\begin{bmatrix} 0 \\ 1/b \\ 0 \end{bmatrix}}_{\boldsymbol{h}_\xi} \underbrace{\begin{bmatrix} 0 \\ 0 \\ -1/b^2 \end{bmatrix}}_{\boldsymbol{h}_v} \begin{bmatrix} \boldsymbol{\chi}_{n,g} \\ \boldsymbol{\xi}_{\chi,n,g} \\ \boldsymbol{v}_{\chi,n,g} \end{bmatrix}. \tag{35}$$

We insert the coordinate transformation (35) and its equivalent for the first augmented TD state into (34) and group the $\boldsymbol{\chi}_{\mathrm{TO},n}$ and $\boldsymbol{\xi}_{\mathrm{TD},1}$ terms on the left-hand side as

$$\underbrace{\begin{bmatrix} \boldsymbol{A}_{N,g}\boldsymbol{h}_\chi & -\boldsymbol{A}_{1,g}\boldsymbol{h}_\xi \end{bmatrix}}_{\boldsymbol{B}_{N,1,g}} \begin{bmatrix} \boldsymbol{\chi}_{n,g} \\ \boldsymbol{\xi}_{\chi,1,g} \end{bmatrix} = -\boldsymbol{A}_{N,g}\boldsymbol{h}_v\boldsymbol{v}_{\chi,n,g} + \boldsymbol{A}_{1,g}\boldsymbol{h}_v\boldsymbol{v}_{\chi,1,g} + \underbrace{\begin{bmatrix} \boldsymbol{A}_1\boldsymbol{h}_\chi & -\boldsymbol{A}_N\boldsymbol{h}_\xi \end{bmatrix}}_{\boldsymbol{B}_{1,N,g}} \begin{bmatrix} \boldsymbol{\chi}_{1,g} \\ \boldsymbol{\xi}_{\chi,n,g} \end{bmatrix} + \boldsymbol{A}_{T,g}\boldsymbol{X}_{\mathrm{ft},g}. \tag{36}$$

To satisfy the VRP continuity constraint, we choose the first and last horizontal foot position to coincide with the respective last VRP of the previous and the first VRP of the next walking sequence, i.e., $\boldsymbol{\chi}_{\mathrm{ft},1,g} = \boldsymbol{v}_{\chi,n,g-1}$ and $\boldsymbol{\chi}_{\mathrm{ft},n,g} = \boldsymbol{v}_{\chi,1,g+1}$. With the first and second row of (14) and (15), we insert into (36) to obtain

$$\begin{aligned} \boldsymbol{B}_{N,1,g} \begin{bmatrix} \boldsymbol{\chi}_{n,g} \\ \boldsymbol{\xi}_{\chi,1,g} \end{bmatrix} &= \boldsymbol{B}_{1,N,g} \begin{bmatrix} \boldsymbol{\chi}_{1,g} \\ \boldsymbol{\xi}_{\chi,n,g} \end{bmatrix} + \\ \underbrace{\left(\boldsymbol{A}_{1,g}\boldsymbol{h}_v\boldsymbol{e}_{n_t,1} - \boldsymbol{A}_{N,g}\boldsymbol{h}_v\boldsymbol{e}_{n_t,n_t} + \boldsymbol{A}_{T,g}\right)}_{\boldsymbol{B}_{T,g}} &\boldsymbol{X}_{\mathrm{ft},g}, \end{aligned} \tag{37}$$

Finally, we find the explicit solution for the final CoM position $\boldsymbol{\chi}_{n,g}$ and first DCM position $\boldsymbol{\xi}_{\chi,1,g}$ as

$$\begin{bmatrix} \boldsymbol{\chi}_{n,g} \\ \boldsymbol{\xi}_{\chi,1,g} \end{bmatrix} = \underbrace{\begin{bmatrix} {}^{\chi}c_{\chi,g} & {}^{\chi}c_{\xi,g} \\ {}^{\xi}c_{\chi,g} & {}^{\xi}c_{\xi,g} \end{bmatrix}}_{\boldsymbol{B}_{N,1,g}^{-1}\boldsymbol{B}_{1,N,g} \in \mathbb{R}^{2\times 2}} \begin{bmatrix} \boldsymbol{\chi}_{1,g} \\ \boldsymbol{\xi}_{\chi,n,g} \end{bmatrix} + \underbrace{\begin{bmatrix} {}^{\chi}\boldsymbol{f}_{t,g} \\ {}^{\xi}\boldsymbol{f}_{t,g} \end{bmatrix}}_{\boldsymbol{B}_{N,1,g}^{-1}\boldsymbol{B}_{T,g} \in \mathbb{R}^{2\times n_t}} \boldsymbol{X}_{\mathrm{ft},g}. \tag{38}$$

Here, the matrices are written in terms of their components to resemble the equation structure shown in (24) for walking.

3) Assembly of the global matrix equation: For the computation of multiple gait sequences, we utilize the common structure of (24) and (38) (see Fig. 3). Our goal is to obtain a matrix equation similar to (4) for computing the waypoints of the entire motion, i.e., the sequences' start and end points, in terms of a global CoM start and DCM target point and the foot positions. First, we alternately select the first rows of (24) and (38), insert (10) and summarize as

$$\boldsymbol{\chi}_g = m_{\chi,g}\boldsymbol{\chi}_{g-1} + n_{\chi,g}\boldsymbol{\xi}_{\chi,g} + \boldsymbol{\tau}_{\chi,g}\boldsymbol{X}_{t,g}, \tag{39}$$

where

$$\left.\begin{aligned} m_{\chi,g} &= {}^{\chi}a_{\chi,g} \\ n_{\chi,g} &= {}^{\chi}a_{\xi,g} \\ \boldsymbol{\tau}_{\chi,g} &= {}^{\chi}\boldsymbol{b}_{t,g} \end{aligned}\right\} \forall g \in g_w, \quad \left.\begin{aligned} m_{\chi,g} &= {}^{\chi}c_{\chi,g} \\ n_{\chi,g} &= {}^{\chi}c_{\xi,g} \\ \boldsymbol{\tau}_{\chi,g} &= {}^{\chi}\boldsymbol{f}_{t,g} \end{aligned}\right\} \forall g \in g_r.$$

Here, the gait sequence target matrix $\boldsymbol{X}_{t,g}$ contains the respective foot positions and we droped the subscripts 1 and n for the CoM and DCM position. Similarly, we alternately select the second rows of (24) and (38) and insert (13) as

$$\boldsymbol{\xi}_{\chi,g} = m_{\xi,g}\boldsymbol{\chi}_g + n_{\xi,g}\boldsymbol{\xi}_{\chi,g+1} + \boldsymbol{\tau}_{\xi,g}\boldsymbol{X}_{t,g}, \tag{40}$$

where

$$\left.\begin{aligned} m_{\xi,g} &= {}^{\xi}a_{\chi,g} \\ n_{\xi,g} &= {}^{\xi}a_{\xi,g} \\ \boldsymbol{\tau}_{\xi,g} &= {}^{\xi}\boldsymbol{b}_{t,g} \end{aligned}\right\} \forall g \in g_w, \quad \left.\begin{aligned} m_{\xi,g} &= {}^{\xi}c_{\chi,g} \\ n_{\xi,g} &= {}^{\xi}c_{\xi,g} \\ \boldsymbol{\tau}_{\xi,g} &= {}^{\xi}\boldsymbol{f}_{t,g} \end{aligned}\right\} \forall g \in g_r.$$

Equations (39) and (40) form a coupled forward and backward recursion that must be solved simultaneously, and thus we adopt the notation from Section II-A to reformulate (39) and (40) in terms of sequence start and end points as

$$\boldsymbol{\chi}_{g,T} = m_{\chi,g}\boldsymbol{\chi}_{g,0} + n_{\chi,g}\boldsymbol{\xi}_{\chi,g,T} + \boldsymbol{\tau}_{\chi,g}\boldsymbol{X}_{t,g}, \tag{41}$$

$$\boldsymbol{\xi}_{\chi,g,0} = m_{\xi,g}\boldsymbol{\chi}_{g,0} + n_{\xi,g}\boldsymbol{\xi}_{\chi,g,T} + \boldsymbol{\tau}_{\xi,g}\boldsymbol{X}_{t,g}, \tag{42}$$

where the subscript 0 denotes start points, e.g., $\boldsymbol{\xi}_{\chi,g,0}$ and the subscript T denotes end points, e.g., $\boldsymbol{\chi}_{g,T}$. We collect the $N = N_g+1$ CoM gait sequence waypoints $\boldsymbol{\chi}_j$ in a matrix $\boldsymbol{X}_G = [\boldsymbol{\chi}_1^{\mathrm{T}} \dots \boldsymbol{\chi}_N^{\mathrm{T}}]^{\mathrm{T}}$ and the DCM gait sequence waypoints $\boldsymbol{\xi}_{\chi,j}$ in a matrix $\boldsymbol{\Xi}_G = [\boldsymbol{\xi}_{\chi,1}^{\mathrm{T}} \dots \boldsymbol{\xi}_{\chi,N}^{\mathrm{T}}]^{\mathrm{T}}$. All foot target positions are combined in the global target matrix $\bar{\boldsymbol{X}}_t = [\boldsymbol{X}_{t,1}^{\mathrm{T}} \dots \boldsymbol{X}_{t,N_g}^{\mathrm{T}}]^{\mathrm{T}}$. With (41) and (42), we can assemble a global matrix equation for the gait sequence waypoints of equivalent structure as (4). We express the global CoM start and DCM target point in terms of $\boldsymbol{X}_G$ and $\boldsymbol{\Xi}_G$ as

$$\boldsymbol{e}_{N,1}\boldsymbol{e}_{N,1}^{\mathrm{T}}\boldsymbol{X}_G = \boldsymbol{e}_{N,1}\bar{\boldsymbol{\chi}}_s, \tag{43}$$

$$\boldsymbol{e}_{N,N}\boldsymbol{e}_{N,N}^{\mathrm{T}}\boldsymbol{\Xi}_G = \boldsymbol{e}_{N,N}\bar{\boldsymbol{\xi}}_{\chi,f}. \tag{44}$$

We define two selection matrices, $\boldsymbol{S}_0 = [\boldsymbol{e}_{N,1} \dots \boldsymbol{e}_{N,N-1}]^{\mathrm{T}}$ and $\boldsymbol{S}_T = [\boldsymbol{e}_{N,2} \dots \boldsymbol{e}_{N,N}]^{\mathrm{T}}$, that select the gait sequence start and end points from the waypoint matrices $\boldsymbol{X}_G$ and $\boldsymbol{\Xi}_G$. The CoM start points $\boldsymbol{X}_{G,0} = \boldsymbol{S}_0\boldsymbol{X}_G$ combine the waypoints $1 \dots N-1$ and the CoM end points $\boldsymbol{X}_{G,T} = \boldsymbol{S}_T\boldsymbol{X}_G$ combine the waypoints $2 \dots N$. The DCM start and end points $\boldsymbol{\Xi}_{G,0}$ and $\boldsymbol{\Xi}_{G,T}$ are defined analogously. Thus we write (41) and (42) in matrix form for N_g gait sequences as

$$\boldsymbol{X}_{G,T} = \boldsymbol{M}_\chi\boldsymbol{X}_{G,0} + \boldsymbol{N}_\chi\boldsymbol{\Xi}_{G,T} + \boldsymbol{T}_\chi\bar{\boldsymbol{X}}_t, \tag{45}$$

$$\boldsymbol{\Xi}_{G,0} = \boldsymbol{M}_\xi\boldsymbol{X}_{G,0} + \boldsymbol{N}_\xi\boldsymbol{\Xi}_{G,T} + \boldsymbol{T}_\xi\bar{\boldsymbol{X}}_t, \tag{46}$$

where $\boldsymbol{M}_\chi$, $\boldsymbol{N}_\chi$, $\boldsymbol{M}_\xi$, and $\boldsymbol{N}_\xi$ are square diagonal matrices whose diagonals contain the coefficients $m_{\chi,g}$, $n_{\chi,g}$, $m_{\xi,g}$, and $n_{\xi,g}$, respectively. The matrices $\boldsymbol{T}_\chi$ and $\boldsymbol{T}_\xi$ are block diagonal matrices whose diagonals contain the vectors $\boldsymbol{\tau}_{\chi,g}$ and $\boldsymbol{\tau}_{\xi,g}$, respectively. Rewriting (45) and (46) in terms of $\boldsymbol{X}_G$ and $\boldsymbol{\Xi}_G$, multiplying from the left by $\boldsymbol{S}_T^{\mathrm{T}}$ and $\boldsymbol{S}_0^{\mathrm{T}}$, respectively, adding (43) and (44), respectively, and combining in a single matrix equation yields

$$\begin{aligned} \underbrace{\begin{bmatrix} \boldsymbol{X}_G \\ \boldsymbol{\Xi}_G \end{bmatrix}}_{\boldsymbol{\Sigma}\in\mathbb{R}^{2N\times 2}} = &\underbrace{\begin{bmatrix} \boldsymbol{S}_T^{\mathrm{T}}\boldsymbol{M}_\chi\boldsymbol{S}_0 & \boldsymbol{S}_T^{\mathrm{T}}\boldsymbol{N}_\chi\boldsymbol{S}_T \\ \boldsymbol{S}_0^{\mathrm{T}}\boldsymbol{M}_\xi\boldsymbol{S}_0 & \boldsymbol{S}_0^{\mathrm{T}}\boldsymbol{N}_\xi\boldsymbol{S}_T \end{bmatrix}}_{\boldsymbol{G}\in\mathbb{R}^{2N\times 2N}} \underbrace{\begin{bmatrix} \boldsymbol{X}_G \\ \boldsymbol{\Xi}_G \end{bmatrix}}_{\boldsymbol{\Sigma}\in\mathbb{R}^{2N\times 2}} \\ &+ \underbrace{\begin{bmatrix} \boldsymbol{S}_T^{\mathrm{T}}\boldsymbol{T}_\chi \\ \boldsymbol{S}_0^{\mathrm{T}}\boldsymbol{T}_\xi \end{bmatrix}}_{\boldsymbol{K}\in\mathbb{R}^{2N\times N_t}} \bar{\boldsymbol{X}}_t + \underbrace{\begin{bmatrix} \boldsymbol{0} \\ \boldsymbol{e}_{N,N} \end{bmatrix}}_{\bar{\boldsymbol{e}}_N\in\mathbb{R}^{2N}} \bar{\boldsymbol{\xi}}_{\chi,f} + \underbrace{\begin{bmatrix} \boldsymbol{e}_{N,1} \\ \boldsymbol{0} \end{bmatrix}}_{\bar{\boldsymbol{e}}_1\in\mathbb{R}^{2N}} \bar{\boldsymbol{\chi}}_s, \end{aligned} \tag{47}$$

where N_t is the total number of target waypoints. The global target matrix $\bar{\boldsymbol{X}}_t$ consists of foot target positions except for the initial and terminal foot position, where different from (23) the respective two horizontal VRP waypoints are chosen to coincide with the midpoint between the two feet. Solving for $\boldsymbol{\Sigma}$ with the initial and terminal constraints (first and second row of (16) and (17)) yields

$$\boldsymbol{\Sigma} = \underbrace{(\boldsymbol{I} - \boldsymbol{G})^{-1}(\boldsymbol{K} + \bar{\boldsymbol{e}}_N \boldsymbol{e}_{N_t,N_t}^{\mathrm{T}} + \bar{\boldsymbol{e}}_1 \boldsymbol{e}_{N_t,1}^{\mathrm{T}})}_{\boldsymbol{U}} \bar{\boldsymbol{X}}_t, \quad (48)$$

where $(\boldsymbol{I} - \boldsymbol{G})^{-1}$ is square, full rank, and thus invertible. Equation (48) is the main result of the horizontal planning. However, we want to satisfy two additional constraints that enable a continuous stand-to-walk transition and a walk-to-stand transition in finite time (without the constraint, the CoM will only converge to the DCM). Thus, we introduce the following constraint equation

$$\begin{bmatrix} \boldsymbol{x}_{n,N_g} \\ \boldsymbol{\xi}_{\chi,1,1} \end{bmatrix} = \underbrace{\begin{bmatrix} \boldsymbol{e}_{N,N}^{\mathrm{T}} & \boldsymbol{0} \\ \boldsymbol{0} & \boldsymbol{e}_{N,1}^{\mathrm{T}} \end{bmatrix} \boldsymbol{U}}_{\boldsymbol{Q} \in \mathbb{R}^{2 \times N_t}} \bar{\boldsymbol{X}}_t \stackrel{!}{=} \underbrace{\begin{bmatrix} \boldsymbol{v}_{\chi,n,N_g} \\ \boldsymbol{v}_{\chi,1,1} \end{bmatrix}}_{\boldsymbol{v}_{\mathrm{des}}}. \quad (49)$$

We choose the second and second-to-last VRP waypoints in $\bar{\boldsymbol{X}}_t$ to satisfy the constraints and solve (49) for these points:

$$\begin{bmatrix} \boldsymbol{v}_{\chi,2,1} \\ \boldsymbol{v}_{\chi,n-1,N_g} \end{bmatrix} = \begin{bmatrix} \boldsymbol{q}_{c2} & \boldsymbol{q}_{cN-1} \end{bmatrix}^{-1} \left(\boldsymbol{v}_{\mathrm{des}} - \boldsymbol{Q}_{\mathrm{rem}} \bar{\boldsymbol{X}}_{t,\mathrm{rem}} \right), \quad (50)$$

where $\boldsymbol{q}_{c2}$ and $\boldsymbol{q}_{cN-1}$ are the second and second-to-last columns of $\boldsymbol{Q}$, and $\boldsymbol{Q}_{\mathrm{rem}}$ and $\bar{\boldsymbol{X}}_{t,\mathrm{rem}}$ are the remaining columns and rows of $\boldsymbol{Q}$ and $\bar{\boldsymbol{X}}_t$, respectively.

By inserting the VRP waypoints from (50) into the global target matrix $\bar{\boldsymbol{X}}_t$ in (48) and solving, we obtain the start and end points of each gait sequence. They are utilized to calculate all waypoints of each gait sequence from which the complete horizontal trajectory can be determined.

IV. Evaluation and Simulation

This section evaluates the proposed methods. Figure 4 shows a series of five consecutive gait sequences with three footsteps each. The robot's CoM motion alternates between walking and running gaits while transitioning from standing to walking and back in the first and last gait sequence, respectively. The VRP, DCM, and CoM trajectories are C^0, C^1, and C^2 continuous, respectively, and consistent in the walk-to-run (W2R) and run-to-walk (R2W) transitions. Although the VRP leaves the footstep region during running, the leg forces line of action always passes through a very narrow area around the foot center, as shown in Fig. 5. During walking single support, the enhanced Centroidal Moment Pivot (eCMP), which encodes external forces (similar to the VRP, see [12]), is stationary in the foot center. During running, it passes below the ground and maintains the force focus. The VRP trajectory results in continuous external forces for the complete trajectory, as shown in Fig. 6.

The pre-planned trajectory is tracked with a combined control approach. Due to the naturally stable CoM dynamics, only the unstable first-order DCM dynamics must

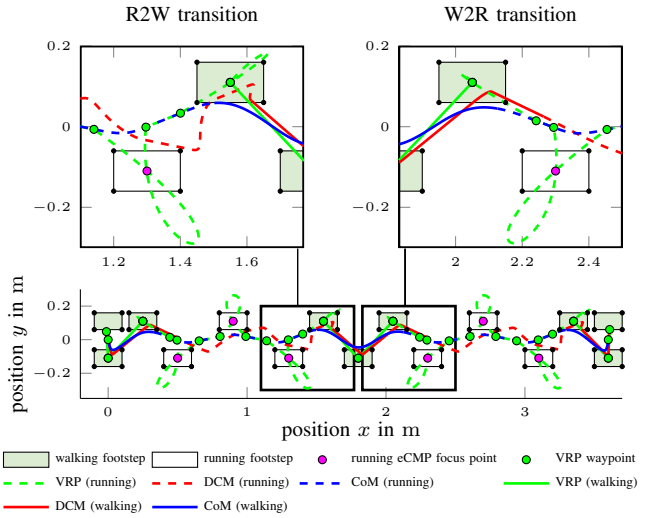

Fig. 4. Top view of a trajectory consisting of five consecutive gait sequences with 0.25 m step length, double support time $T_{\mathrm{DS}} = 0.12\,\mathrm{s}$, and single support time $T_{\mathrm{SS}} = 0.6\,\mathrm{s}$ during walking and 0.4 m step length and stance time $T_s = 0.12\,\mathrm{s}$ during running.

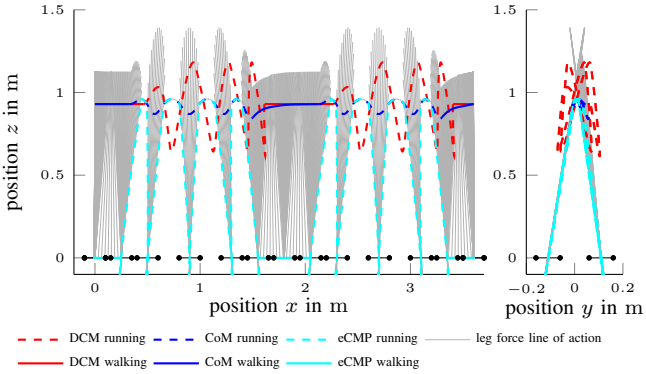

Fig. 5. Side view of the trajectory in x- and y-direction highlights the focus of external forces in the foot center. For visibility, only running sequences are displayed in the plot on the right.

be controlled. The DCM control framework used for this purpose is adopted from [25]. The trajectory generation and DCM controller are integrated into an inverse dynamics-based whole-body control (WBC) framework, which has been shown to provide satisfactory results for both gaits individually [12], [20]. The simulations are performed in Matlab/Simulink, which is linked to the OpenHRP [27] simulation platform. Fig. 1 shows snapshots of the transition from walking to running of the humanoid robot Toro in simulation for time intervals of 0.2 s. The plot starts at the end of the last walking double support phase at $t = 0\,\mathrm{s}$ and the gait transition occurs in the last single support phase at $t = 0.4\,\mathrm{s}$. The DCM and CoM reference trajectories compared to the actual values calculated in the whole-body simulation are shown in Fig. 7 and demonstrate satisfactory tracking with minimal deviations in the walking sequences. We can observe an increasing CoM tracking error in the running sequences while the DCM tracking performance stays constant. This highlights the importance of online re-planning of the trajectory based on state measurements.

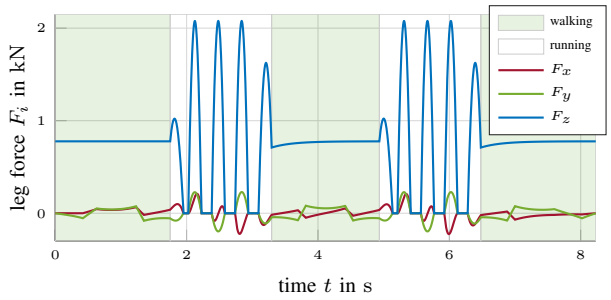

Fig. 6. Leg forces over time of the humanoid robot Toro ($m = 79.2\,\mathrm{kg}$). Step lengths and timings according to Fig. 4.

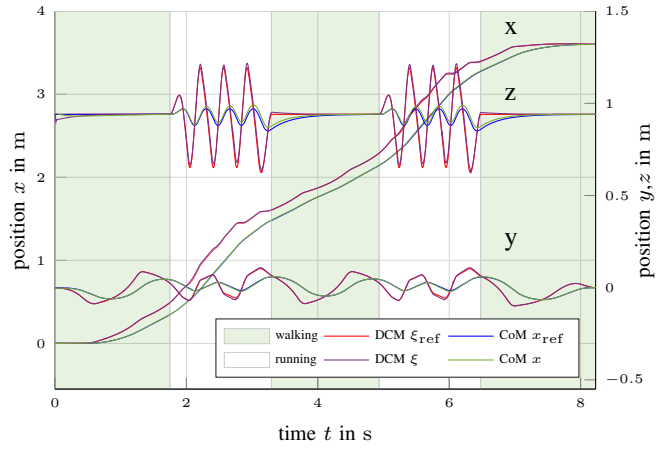

Fig. 7. CoM and DCM reference trajectories compared to values from a simulation of the humanoid Toro [4] following the trajectory from Fig. 4.

V. Conclusion and Future Work

This paper presented an analytical trajectory generator for gait transitions between walking and running. We showed that the proposed framework combines two significantly different planning approaches to produce a consistent CoM trajectory for the two gaits. The method was verified in a whole-body simulation with the humanoid robot Toro.

Future research will focus on online re-planning of the trajectory based on state measurements to react to disturbances. Furthermore, the gait parameters, i.e., stance times, apex height, and step length, will be adjusted depending on the current locomotion velocity to obtain a more natural and human-like gait. Finally, we plan to experimentally evaluate the presented methods on a humanoid robot.

References

[1] S. Cotton *et al.*, "Multi-Legged Running Robot," US Patent US20 160 001 831A1, 2016.

[2] D. W. Haldane, J. K. Yim, and R. S. Fearing, "Repetitive extreme-acceleration (14-g) spatial jumping with Salto-1P," in *Proc. IEEE/RSJ Int. Conf. Intell. Robots Syst.*, 2017, pp. 3345–3351.

[3] C. R. Lee and C. T. Farley, "Determinants of the center of mass trajectory in human walking and running." *Journal of Experimental Biology*, vol. 201, no. 21, pp. 2935–2944, 1998.

[4] J. Englsberger *et al.*, "Overview of the torque-controlled humanoid robot TORO," in *Proc. IEEE-RAS 15th Int. Conf. Humanoid Robots*, 2014, pp. 916–923.

[5] S. Kajita, F. Kanehiro, K. Kaneko, K. Yokoi, and H. Hirukawa, "The 3D linear inverted pendulum mode: A simple modeling for a biped walking pattern generation," in *Proc. IEEE Int. Conf. Robot. Automat.*, vol. 1, 2001, pp. 239–246.

[6] T. Sugihara, Y. Nakamura, and H. Inoue, "Real-time humanoid motion generation through ZMP manipulation based on inverted pendulum control," in *Proc. IEEE Int. Conf. Robot. Automat.*, vol. 2, 2002, pp. 1404–1409.

[7] R. Tedrake, S. Kuindersma, R. Deits, and K. Miura, "A closed-form solution for real-time ZMP gait generation and feedback stabilization," in *Proc. IEEE-RAS 15th Int. Conf. Humanoid Robots*, 2015, pp. 936–940.

[8] T. Takenaka, T. Matsumoto, and T. Yoshiike, "Real time motion generation and control for biped robot -1st report: Walking gait pattern generation-," in *Proc. IEEE/RSJ Int. Conf. Intell. Robots Syst.*, 2009, pp. 1084–1091.

[9] J. Pratt, J. Carff, S. Drakunov, and A. Goswami, "Capture Point: A Step toward Humanoid Push Recovery," in *Proc. IEEE-RAS 15th Int. Conf. Humanoid Robots*, 2006, pp. 200–207.

[10] J. Englsberger, C. Ott, M. A. Roa, A. Albu-Schäffer, and G. Hirzinger, "Bipedal walking control based on Capture Point dynamics," in *Proc. IEEE/RSJ Int. Conf. Intell. Robots Syst.*, 2011, pp. 4420–4427.

[11] T. Koolen, T. de Boer, J. Rebula, A. Goswami, and J. Pratt, "Capturability-based analysis and control of legged locomotion, Part 1: Theory and application to three simple gait models," *Int. J. Robot. Res.*, vol. 31, no. 9, pp. 1094–1113, Aug. 2012.

[12] J. Englsberger, G. Mesesan, and C. Ott, "Smooth trajectory generation and push-recovery based on Divergent Component of Motion," in *Proc. IEEE/RSJ Int. Conf. Intell. Robots Syst.*, 2017, pp. 4560–4567.

[13] S. Kajita, T. Nagasaki, K. Yokoi, K. Kaneko, and K. Tanie, "Running pattern generation for a humanoid robot," in *Proc. IEEE Int. Conf. Robot. Automat.*, vol. 3, 2002, pp. 2755–2761.

[14] T. Nagasaki, S. Kajita, K. Yokoi, K. Kaneko, and K. Tanie, "Running pattern generation and its evaluation using a realistic humanoid model," in *Proc. IEEE Int. Conf. Robot. Automat.*, vol. 1, 2003, pp. 1336–1342.

[15] T. Takenaka, T. Matsumoto, T. Yoshiike, and S. Shirokura, "Real time motion generation and control for biped robot -2nd report: Running gait pattern generation-," in *Proc. IEEE/RSJ Int. Conf. Intell. Robots Syst.*, 2009, pp. 1092–1099.

[16] H. Geyer, A. Seyfarth, and R. Blickhan, "Compliant leg behaviour explains basic dynamics of walking and running," *Proc. Royal Soc. B: Biological Sciences*, vol. 273, no. 1603, pp. 2861–2867, 2006.

[17] A. Wu and H. Geyer, "The 3-D Spring–Mass Model Reveals a Time-Based Deadbeat Control for Highly Robust Running and Steering in Uncertain Environments," *IEEE Trans. Robot.*, vol. 29, no. 5, pp. 1114–1124, 2013.

[18] P. M. Wensing and D. E. Orin, "High-speed humanoid running through control with a 3D-SLIP model," in *Proc. IEEE/RSJ Int. Conf. Intell. Robots Syst.*, 2013, pp. 5134–5140.

[19] B. Dadashzadeh, H. R. Vejdani, and J. Hurst, "From template to anchor: A novel control strategy for spring-mass running of bipedal robots," in *Proc. IEEE/RSJ Int. Conf. Intell. Robots Syst.*, 2014, pp. 2566–2571.

[20] J. Englsberger, P. Kozłowski, C. Ott, and A. Albu-Schäffer, "Biologically Inspired Deadbeat Control for Running: From Human Analysis to Humanoid Control and Back," *IEEE Trans. Robot.*, vol. 32, no. 4, pp. 854–867, 2016.

[21] J. Rummel, Y. Blum, and A. Seyfarth, "From Walking to Running," in *Autonome Mobile Systeme 2009*, 2009, pp. 89–96.

[22] T. Kamioka *et al.*, "Dynamic gait transition between walking, running and hopping for push recovery," in *Proc. IEEE-RAS 15th Int. Conf. Humanoid Robots*, 2017, pp. 1–8.

[23] T. Sugihara, K. Imanishi, T. Yamamoto, and S. Caron, "3D biped locomotion control including seamless transition between walking and running via 3D ZMP manipulation," in *Proc. IEEE Int. Conf. Robot. Automat.*, 2021, pp. 6258–6263.

[24] F. M. Smaldone, N. Scianca, L. Lanari, and G. Oriolo, "From Walking to Running: 3D Humanoid Gait Generation via MPC," *Frontiers in Robotics and AI*, to be published.

[25] J. Englsberger, C. Ott, and A. Albu-Schäffer, "Three-Dimensional Bipedal Walking Control Based on Divergent Component of Motion," *IEEE Trans. Robot.*, vol. 31, no. 2, pp. 355–368, 2015.

[26] G. Mesesan, J. Englsberger, C. Ott, and A. Albu-Schäffer, "Convex Properties of Center-of-Mass Trajectories for Locomotion Based on Divergent Component of Motion," *IEEE Robotics and Automation Letters*, vol. 3, no. 4, pp. 3449–3456, 2018.

[27] F. Kanehiro *et al.*, "Open architecture humanoid robotics platform," *Proc. IEEE Int. Conf. Robot. Automat.*, 2002.